Journal of Alloys and Compounds 1065 (2026) 188036

Contents lists available at ScienceDirect

Journal of Alloys and Compounds

journal homepage: www.elsevier.com/locate/jalcom

Influence of point defects on the hardness and reduced modulus of B2-ordered FeAl

Jung Soo Lee [a,*], Jan Lars Riedel [b], Peter Schweizer [a], Alexander Kauffmann [c], Martin Heilmaier [b], Gerhard Dehm [a], James P. Best [a], Anwesha Kanjilal [a,*], Frank Stein [a,*]

[a] Max Planck Institute for Sustainable Materials, Düsseldorf 40237, Germany
[b] Institute for Applied Materials (IAM), Karlsruhe Institute of Technology (KIT), Karlsruhe 76131, Germany
[c] Institute for Materials (IM), Ruhr University Bochum (RUB), Bochum 44801, Germany

ARTICLE INFO

Keywords:
B2-ordered FeAl
Nanoindentation
Hardness
Reduced modulus
Vacancies
Anti-site defects

ABSTRACT

B2-ordered FeAl exhibits a wide homogeneity range (from 23.5 to 53 at.% Al) and a strong sensitivity of its mechanical properties to point defects, but the individual roles of vacancies and anti-site atoms remain insufficiently clarified. In this work, we investigate how these defects influence hardness and reduced modulus across the full single-phase composition range of B2-ordered FeAl. For this purpose, diffusion couples between two Fe-Al alloys with 30 and 53 at.% Al were prepared and mechanical properties were studied by nanoindentation. Diffusion bonding at 1000 °C followed by various heat treatments at 400–1000 °C is employed to systematically vary the concentration of quenched-in vacancies, while anti-site defect concentrations are primarily dictated by composition. Nanoindentation along the composition gradient reveals that low-vacancy states exhibit a non-monotonic hardness–composition behavior with a distinct minimum in hardness, whereas high-vacancy states show a monotonic increase in hardness with increasing Al content. Comparison of differently heat-treated conditions demonstrates that such trends can be explained by the combined effects of vacancies and anti-site defects, where vacancy hardening is known to be most pronounced near stoichiometric B2-ordered FeAl, while anti-site defect strengthening dominates on the Fe-rich side of the composition range. The composition dependence of the reduced modulus likewise changes with heat treatment, indicating that point defects also affect elastic stiffness. Together, these results provide a coherent experimental understanding of how vacancies and anti-site defects jointly control the mechanical response of B2-ordered FeAl and help rationalize previously reported anomalies in the composition-dependent properties.

1. Introduction

Alloys based on B2-ordered FeAl have attracted attention for many years as potential structural materials for intermediate- to high-temperature applications owing to their low density, good oxidation and sulfidation resistance, and cost efficiency compared to Ni-, and Co-based alloys and high-temperature steels [1–5]. Moreover, interesting ideas have also been developed for applications of B2-ordered FeAl as functional material for magnetic recording and data storage [6]. However, the industrial application of B2-ordered FeAl alloys, particularly for structural applications, is impeded by their low ductility at ambient temperatures and their overall very complex and not fully understood mechanical behavior [3,4,7,8]. The B2-ordered FeAl phase possesses a wide homogeneity range from 23.5 to 53 at.% Al as shown in Fig. 1a (adapted from [9]). The deviations from its stoichiometric composition of 50 at.% are accommodated by vacancies and anti-site atoms [7,10]. Interestingly, it was observed in several studies that the mechanical properties of single-phase B2-ordered FeAl alloys can exhibit an unexpected behavior when examined as a function of composition. Properties such as hardness, lattice resistance, Hall-Petch slope, and brittle-to-ductile transition temperature show an abrupt change or a minimum at a certain composition somewhere in the wide homogeneity range of the phase, which, in addition, seems to depend on the thermal history of the material [7,11–13].

The mechanical properties of ordered phases are strongly influenced by defects, which can be simple point defects as well as higher-dimensional defects such as antiphase boundaries (APBs) or grain boundaries [8,14,15]. One of the most well-studied effects of point

* Corresponding authors.
E-mail addresses: js.lee@mpi-susmat.de (J.S. Lee), a.kanjilal@mpi-susmat.de (A. Kanjilal), f.stein@mpi-susmat.de (F. Stein).

https://doi.org/10.1016/j.jallcom.2026.188036
Received 11 February 2026; Received in revised form 1 April 2026; Accepted 13 April 2026
Available online 14 April 2026

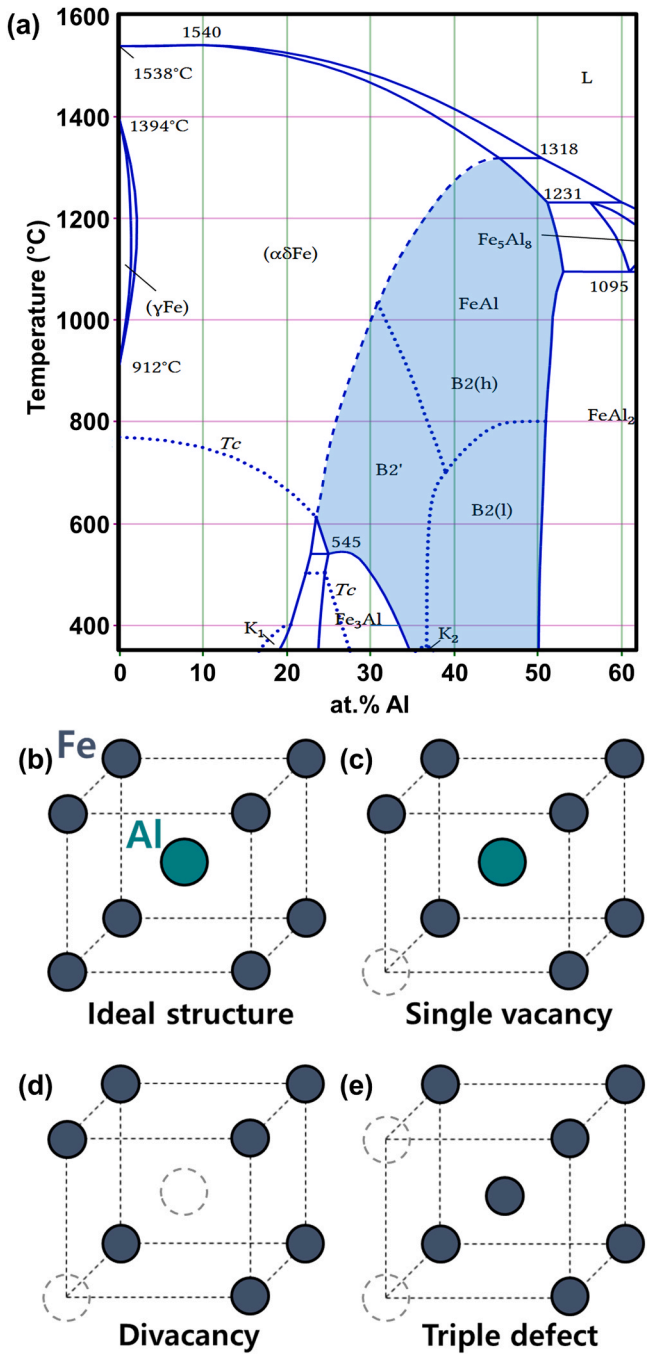

Fig. 1. (a) Fe-rich part of the Fe-Al phase diagram adapted from Ref. [9]. The blue region is the single phase B2-ordered FeAl region. Schematic diagrams of B2-ordered FeAl lattice with: (b) ideal structure, (c) single vacancy, (d) divacancy (one Fe- and one Al-vacancy), and (e) triple defect (comprising of two Fe-vacancies and an Fe-anti-site defect); the vacancies in (c), (d), and (e) are indicated by dashed circles.

defects in B2-ordered FeAl is the mechanism of vacancy strengthening/hardening [16–21]. The presence of a vacancy inside a crystal lattice creates a local distortion and the interaction between the resulting stress field and a moving dislocation results in strengthening which is comparable to the mechanism of solid solution strengthening [19,22]. The concentration of vacancies at the stoichiometric composition reaches high values at high temperatures (for example, approximately 2% at 1000 °C [23,24]), while these values strongly decrease with decreasing Al content as was found experimentally [19,25–27] and confirmed in several theoretical studies [28–30]. Chang *et al.* [18] have shown that the microhardness increases linearly with the square root of the vacancy concentration in B2-ordered FeAl. This was further confirmed in later studies as well [31,32]. The other important type of point defects in B2-ordered FeAl are anti-site defects (i.e., Fe on Al sites). They have also been attributed to contribute to strengthening in B2-ordered FeAl, although less strongly than vacancies [18,19,33]. In contrast to vacancies, their concentration increases with deviation from the stoichiometric composition, i.e., there is a continuous, approximately linear increase with decreasing Al content [27,34]. Besides point defects, anti-phase boundaries (APBs) are known to strengthen crystallographically ordered materials by hindering dislocation motion [35,36]. However, in the case of B2-ordered FeAl, it has been found that APBs do not contribute to strengthening [37]. According to TEM and DFT studies of Hillel *et al.* [38], APBs may occur in B2 FeAl only for Al concentrations < 32 at.%, while for higher Al contents dislocations are observed. These dislocations, which also act as sinks for thermal vacancies during annealing, lead to only minor hardening that is negligible compared to the effects of vacancies and anti-site defects [39].

The most important factor responsible for the complex mechanical behavior of B2 FeAl alloys is the high sensitivity to the concentration, type, and stability of defects, which are influenced by the composition and processing conditions. The thermal vacancies formed at high temperatures can be retained at room temperature upon quenching [23,25,32,40], allowing the mechanical properties to be investigated not only as a function of composition, but also for fixed compositions as a function of different concentrations of quenched-in vacancies. The reason why vacancies can be quenched-in from high temperatures is that the formation enthalpies are relatively low (0.65–1.2 eV) [4,41] and the migration enthalpies are relatively high (1.5–1.8 eV) [41] which makes diffusion sluggish. In contrast, the concentration of anti-site defects measured at room temperature does not depend on the temperature from which an alloy has been quenched [34]. Thus, varying the heat-treatment conditions of the samples provides a pathway to separate the effects of the vacancies from those of the anti-site atoms on the mechanical properties.

Another key feature of B2-ordered FeAl is that vacancies and anti-site atoms can agglomerate to form complex defects such as divacancies (pairs of vacancies) and triple defects (combinations of two Fe vacancies and one Fe anti-site atom [42]) depending on temperature and composition. Schematic diagrams of the ideal B2 unit cell, a single vacancy, a divacancy, and a triple defect are shown in Fig. 1b-e. According to the phase diagram (Fig. 1a), the B2 FeAl single-phase region is subdivided into three different parts. This subdivision of the phase field originates from the early work of Köster and Gödecke [43], who observed sudden changes in thermal expansion and elastic modulus measurements at these compositions and temperatures. Later on, Hehenkamp *et al.* [23] assigned different preferred defect arrangements to these three B2 phase fields using differential dilatometry and positron annihilation spectroscopy. According to their interpretation, single vacancies dominate in the composition range below approximately 35 at.% Al, designated as B2' region in the phase diagram in Fig. 1a, while at higher Al contents triple defects form as the dominant type of defect in the B2(l) region, and at high temperatures above approximately 800 °C in the B2(h) region, divacancies (combination of Fe + Al vacancy) exist in addition. A similar interpretation was given by Haraguchi *et al.* [44,45], while according to other groups [42,46], triple defects dominate in the high-temperature range (above 800 °C) and single vacancies with temperature dependent concentration of triple defects are present at lower temperatures [42,46]. Regardless of these varying interpretations and although the boundaries subdividing the B2 phase field are not precisely defined, also many other studies [9,47–49] agree that different (combinations of) defect variants dominate in the different composition and temperature regions of the extended phase field of B2-ordered FeAl. Since the defect concentration is also strongly influenced by the thermal history of the sample, and because the mechanical behavior is highly sensitive to the defect state, it can be assumed that the complex and, in

some cases, not yet fully understood composition dependence of the mechanical properties of B2-ordered FeAl alloys is related to the respective defect state of the material.

Apart from the hardness and yield strength, which are strongly influenced by the defect concentration as has already been observed in many studies [16–21,33], the experimentally determined elastic modulus of B2-ordered FeAl is known to increase from Fe-rich compositions up to approximately 35–45 at.% Al and then either decreases or remains almost constant [12,50–54]. However, the effects of different heat treatments and point defect concentrations on the elastic modulus have not been systematically studied yet.

Therefore, this work aims to investigate the influence of point defects, specifically vacancies and anti-site atoms, on the mechanical properties of B2-ordered FeAl across its entire single-phase composition range. To this end, the diffusion couple technique has been employed to produce the samples, enabling the entire B2-ordered FeAl composition range to be studied within a single specimen. This approach offers clear advantages over testing series of separate bulk alloys, as it allows property measurements along the continuous concentration gradient at any composition and in finely spaced compositional intervals without the need to cast each composition individually. Furthermore, it ensures that all compositions experience identical heat-treatment conditions (atmosphere, temperature, duration, and cooling), thereby eliminating sample-to-sample variations in fabrication. Moreover, the impurity contents are identical for all compositions. Hence, this work for the first time studies the aforementioned effects and correlations in a single specimen. The unfortunate drawback of utilizing diffusion couples is that the available techniques for characterizing point defects (such as positron annihilation spectroscopy, dilatometry, X-ray diffraction etc.) cannot be employed, as the specimen's compositional gradient necessitates the use of a local probe technique. Hence, we compare the point defect concentrations by an indirect and qualitative method. For our experiments, heat treatments at different temperatures varying from 400 to 1000 °C followed by water quenching were carried out to produce different concentrations of vacancies. 400 °C was chosen as the lower limit for the heat treatments because it has been reported in the literature that heat treatments at this temperature (for at least 100 h) can produce the minimum vacancy concentration state [16]. Subsequently, nanoindentation was performed to locally measure the mechanical properties, thereby probing the intrinsic response of a specific composition without the influence of grain boundaries. It is important to decouple the grain boundary effects from the bulk response as the characteristics and behavior of grain boundaries also depend on the composition [11,55] and can obscure the intrinsic mechanical response from the lattice. For example, the elongation to fracture decreases [55] and the brittle-to-ductile transition temperature of polycrystalline B2 FeAl alloys increases abruptly [11] with increasing Al content. This is accompanied by a change of the fracture mode from transgranular to intergranular. In this study, the reduced modulus and hardness obtained from nanoindentation were analyzed as indicators of elastic and plastic materials' response insensitive to changes in grain boundary properties. Studying the effects of different heat treatments on hardness and reduced modulus enables us to disentangle the contributions of different point defects on the mechanical properties as a function of Al content.

2. Experimental procedure

2.1. Fabrication of diffusion couples

Two binary alloys with compositions Fe-30 and 53 at.% Al were produced by melting the pure metals in a vacuum induction furnace and then casting into copper moulds. Chemical analysis of the as-cast material revealed low impurity contents of < 100 ppm by weight for O, N, C, and S in both alloys (a more detailed description of the analyses and results are given elsewhere [56]). The cast ingots were cut using electrical discharge machining into cuboidal samples with dimensions of $10 \times 5 \times 5$ mm^3. They were ground up to grit P1000 and polished to remove any oxide formed during machining. Especially, the sides which were going to make contact to form the diffusion couple interfaces were ground up to grit P4000 SiC paper. One of each prepared alloy samples was placed on top of one another and carefully placed between disc-shaped molybdenum clamps. Rock wool was placed between the molybdenum clamps and the Fe-Al samples to avoid direct contact between them and prevent any chemical interaction between the two. The clamps were tightened using stainless steel screws and nuts. The entire set was encapsulated inside a quartz ampoule that also had titanium getter and was filled with argon gas. This encapsulated assembly was then heat treated in a furnace at 1000 °C for 240 h, followed by furnace cooling.

2.2. Heat treatment of diffusion couples

The diffusion couples produced as described above were cut into thinner samples with dimensions of approximately $10 \times 5 \times 2$ mm^3 using a diamond wire saw cutting machine. They were polished to remove any surface oxide layer formed during the diffusion bonding process using grit P1000 SiC paper. The diffusion couples were then wrapped in niobium foils to avoid direct contact with the quartz ampoules and were encapsulated in a similar manner as mentioned in Section 2.1. Heat treatments of these samples were carried out as listed in Table 1. All heat treatments were followed by water quenching.

2.3. Sample preparation for microstructural characterization and mechanical property measurement

The furnace-cooled and heat-treated diffusion couples were prepared for further experiments and investigations by polishing them down to a 1 μm finish using a diamond suspension, followed by electropolishing using Struers A2 electrolyte.

2.4. Microstructure analysis

The microstructures of the diffusion couples were investigated using a Zeiss Auriga scanning electron microscope (SEM) that is also equipped with an EDAX TSL-OIM system for electron backscatter diffraction (EBSD). EBSD was performed to determine the orientation and size of the grains.

Transmission electron microscopy (TEM) was performed using a Thermo Fisher Scientific Titan Themis G2 60–300 at 300 keV energy to identify the ordering state and check the presence of dislocations and APBs. Samples for TEM were produced by both twin-jet electropolishing using electrolyte containing 90% acetic acid and 10% perchloric acid, as well as using a Thermo Fisher Scientific Scios 2 focused ion beam instrument.

2.5. Nanoindentation

Nanoindentation was performed on the diffusion couples using a G200 nanoindenter from KLA Corporation. A diamond Berkovich

Table 1
Heat treatments of the diffusion couples after the diffusion bonding process (at 1000 °C/240 h with subsequent furnace cooling (FC)). All samples were water quenched after the heat treatments.

Heat treatment notation	Temperature (°C)	Duration (h)
FC/400-24	400	24
FC/400-168	400	168
FC/400-1008	400	1008
FC/550-168	550	168
FC/700-24	700	24
FC/900-24	900	24
FC/1000-24	1000	24

indenter was used to indent up to a maximum depth of 1 μm, avoiding the indentation size effect, at a constant strain rate of 0.02 s^{-1}. An indentation array layout of five lines with 60 indents in each line was used along the concentration gradient of each diffusion couple. A distance of 30 μm was maintained between the lines of indents, which is greater than 25 times of the maximum indentation depth to avoid interactions between the plastically deformed volume surrounding the indents. The distance between the adjacent indents in each line was maintained at 100 μm.

The Oliver-Pharr method [57] was used to determine the hardness and reduced modulus from the unloading curves. The reduced modulus (E_r) incorporates the elastic response of both the indenter and the specimen according to the following equation:

$$\frac{1}{E_r} = \frac{1-\upsilon^2}{E} + \frac{1-\upsilon_i^2}{E_i} \quad (1)$$

where E is the elastic modulus of the specimen, E_i is the elastic modulus of the indenter tip, ν is the Poisson's ratio of the specimen, and ν_i is the Poisson's ratio of the indenter tip. This equation is valid under the assumption that the material is isotropic. However, B2-ordered FeAl is elastically anisotropic [50,51]. Moreover, because the Poisson's ratios of the compositions under investigation (approximately from 30 to 53 at.% Al) are not known, the values of the reduced modulus were used in this study. Due to the constant and much higher modulus of the diamond indenter as compared to the sample, the contribution of the second term due to the indenter in Eq. 1 will be small and constant. Consequently, changes in the reduced modulus directly reflect changes in the specimen's elastic modulus. Therefore, the composition dependence of the reduced modulus can be interpreted as representing the composition dependence of the elastic modulus of FeAl.

2.6. Composition analysis

Following nanoindentation, the composition profiles of the diffusion couples were measured along the concentration gradient using an electron probe microanalyzer (EPMA) JXA-iSP100 from JEOL at 15 kV voltage and 20 nA beam current. The measurements were performed parallel to the indentation rows with probe points located approximately 10 μm away from the indents in order to determine the local composition at each indentation site.

3. Results

3.1. Microstructure

Fig. 2a shows the overall microstructure, while Fig. 2b shows an EBSD grain-orientation map of an indented area of the FC diffusion couple near the clearly visible diffusion interface. The microstructure exhibits grains with grain sizes in the order of several hundred micrometers to millimeters. Towards the Al-rich side of the diffusion couple (which lies outside the area visible in Fig. 2a), fine $FeAl_2$ phase particles precipitate (see Fig. S1a in Supplementary Information), corroborating the Al-rich boundary of the B2 FeAl single-phase field, which according to the Fe-Al phase diagram is around 50 at.% Al. In the Fe-rich regions (below approximately 36 at.% Al) of diffusion couples annealed at low temperatures (400 and 550 °C), very fine and widely spaced needle-shaped Fe_3AlC precipitates with a length of up to approximately 4 μm and width below about 0.1 μm were observed (as shown in Fig. S1b in Supplementary Information). The occurrence of such fine carbide precipitates is well-known from the literature, and they already form for C contents as low as 80 wt.ppm in Fe-rich alloys [58].

It should also be mentioned that $D0_3$-ordering was observed at 30 at.% Al in the FC/400–1008 diffusion couple (see the TEM results shown in the Supplementary Information Fig. S2). This is in agreement with the phase diagram (see Fig. 1a), according to which at 400 °C, the $D0_3$-ordered superstructure phase Fe_3Al forms between 30–33 at.% Al, while B2 ordering is retained for higher Al contents. In agreement with this, a 400°C heat-treated sample with 35 at.% Al did not show any indication of $D0_3$-ordering but was found to be entirely B2-ordered (see Fig. S2 in the Supplementary Information). For 30 at.% Al heat treated at 1000 °C, the fast second-order phase transformation from B2 to $D0_3$-ordering could not be completely inhibited by water-quenching. This resulted in very fine and homogeneous mixture of B2 and $D0_3$-ordering within the sample. Hence, the diffusion couple, that was quenched from the high-temperature B2-ordered state and has compositions in the $D0_3$ range, will have such a microstructure. Moreover, the samples were checked for the presence of dislocations and APBs. The dislocation densities could be estimated to be in the order of 10^{12}–10^{13} m^{-2} in all cases and there is no visible significant difference for different compositions and for different heat treatments (see also the representative TEM bright field images in Fig. S3 in the Supplementary Information). While APBs were confirmed at 35 (400 and 1000 °C) and 37 (400 °C) at.% Al, none were observed at 42 at.% (400 °C) Al. The appearance and number of APBs in the 400 and 1000 °C TEM samples were very similar. Although this is not a detailed analysis, it is reasonable to conclude that the differences in the hardness arising from different heat treatments and from changes in composition are not as a result of these 1- or 2-dimensional defects.

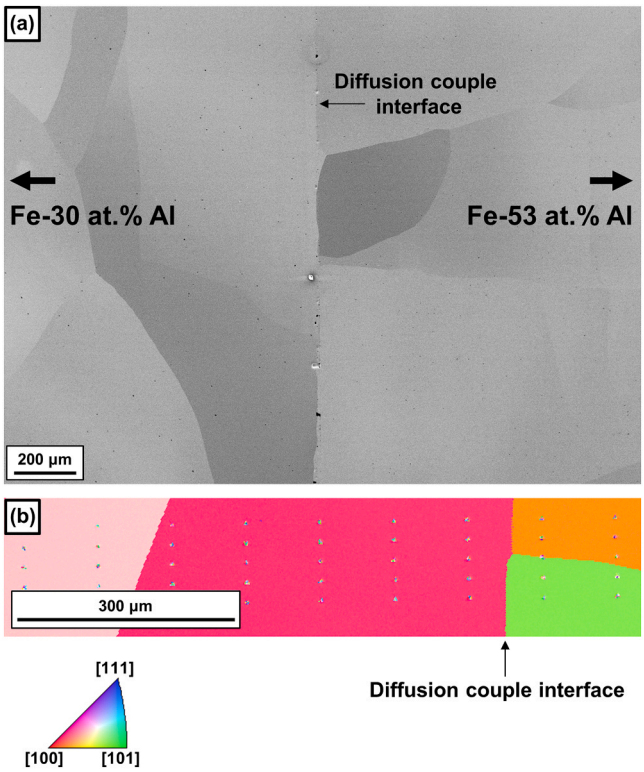

Fig. 2. (a) Low magnification secondary electron image of the central part of a FC diffusion couple including the diffusion couple interface (b) EBSD grain-orientation map of an indented region, not shown in (a), of the same sample near the diffusion couple interface. The color code corresponds to the inverse pole figure of the indentation direction.

3.2. Composition profiles

Fig. 3a and b show the composition profiles as a function of distance of the FC and FC/700–24 heat-treated diffusion couples, and Fig. 3c shows an SEM image of indents and the corresponding EPMA measurement spots. It can be observed from the figure that the samples have well diffusion-bonded, resulting in a sigmoidal shape of the Al

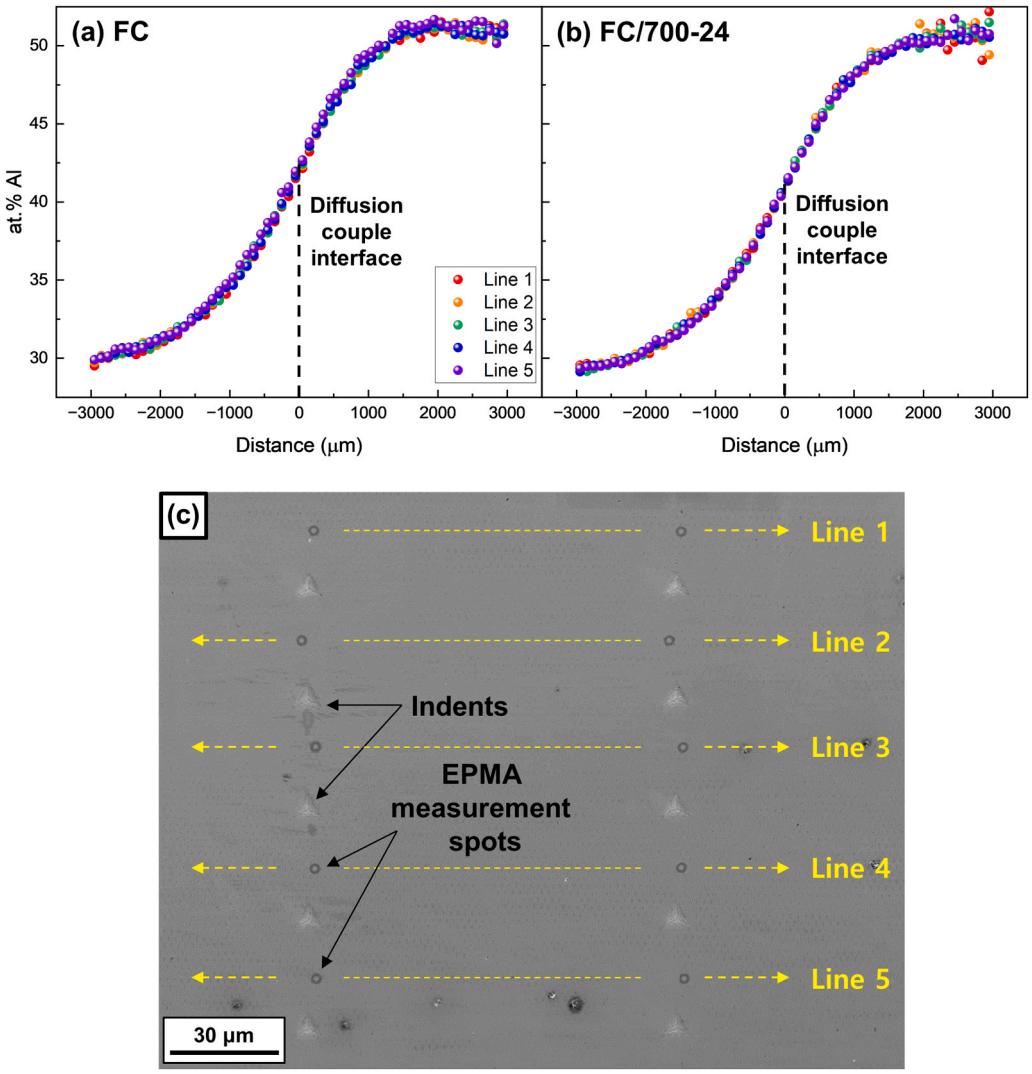

Fig. 3. Composition profiles of (a) FC and (b) FC/700-24 diffusion couples measured using EPMA, and (c) secondary electron image showing the indents together with corresponding EPMA measurement spots, which were positioned approximately 10 μm above the indents. The profiles shown in (a) and (b) are superpositions of the composition values of five line scans each measured parallel to the concentration gradient (which is in horizontal direction in (c)).

concentration profile as a function of the distance perpendicular to the diffusion couple interface. The concentration profile extends over several millimeters and covers the FeAl composition range from 30 to 53 at.% Al. The composition profile remains virtually unchanged after the additional heat treatments (as can be clearly seen in Fig. 3a and b), since the applied temperature-time combinations only result in negligible long-range diffusional processes compared to the initial diffusion bonding treatment of 240 h at 1000 °C. The maximum concentration gradient, which corresponds to the steepest part of the profile near the diffusion couple interface, is approximately 0.01 at.%/μm. Such a small composition variation is sufficiently minor to exclude potential effects of compositional variations on a single nanoindentation measurement where only small localized regions (with plastic zone size radius of the produced indents being less than 6 μm, as estimated according to the modified Nix-Gao model [59,60]) are probed.

3.3. Nanoindentation

3.3.1. Hardness

The hardness obtained from nanoindentation is plotted in Fig. 4 for each heat-treatment condition as a function of the Al content. Some of the representative load-displacement curves are shown in the Supplementary Information Fig. S4. The hardness plot of the FC condition reveals a gradual decrease followed by a rather steep increase in hardness with increasing Al content, resulting in a minimum in the hardness at approximately 42 at.% Al. Such a trend is also observed after the additional heat treatments at lower temperatures, namely, FC/550–168, FC/400–24, −168 and −1008. The steep increase in hardness at higher Al concentrations was already reported in earlier studies where samples were furnace-cooled very slowly from high temperature (1000 °C) and then heat treated at low temperatures (300–500 °C) [12,16,18]. However, in these studies, bulk alloys with different compositions were used instead of diffusion couples, and the existence of a hardness minimum could not be clearly observed, probably because of the rather large composition difference between the consecutive compositions of alloys investigated.

The present measurements further show that the composition at which the minimum in the hardness curves occurs also depends on the heat-treatment parameters. While it occurs at about 42 at.% Al in the FC condition, the minimum is shifted towards higher Al content of about 43 at.% after the heat treatments FC/550–168 and FC/400–24, and further to about 47 at.% Al after the prolonged heat treatments FC/400–168 and FC/400–1008. In contrast, the heat treatments at higher temperatures (FC/700–24, FC/900–24, and FC/1000–24) do not result

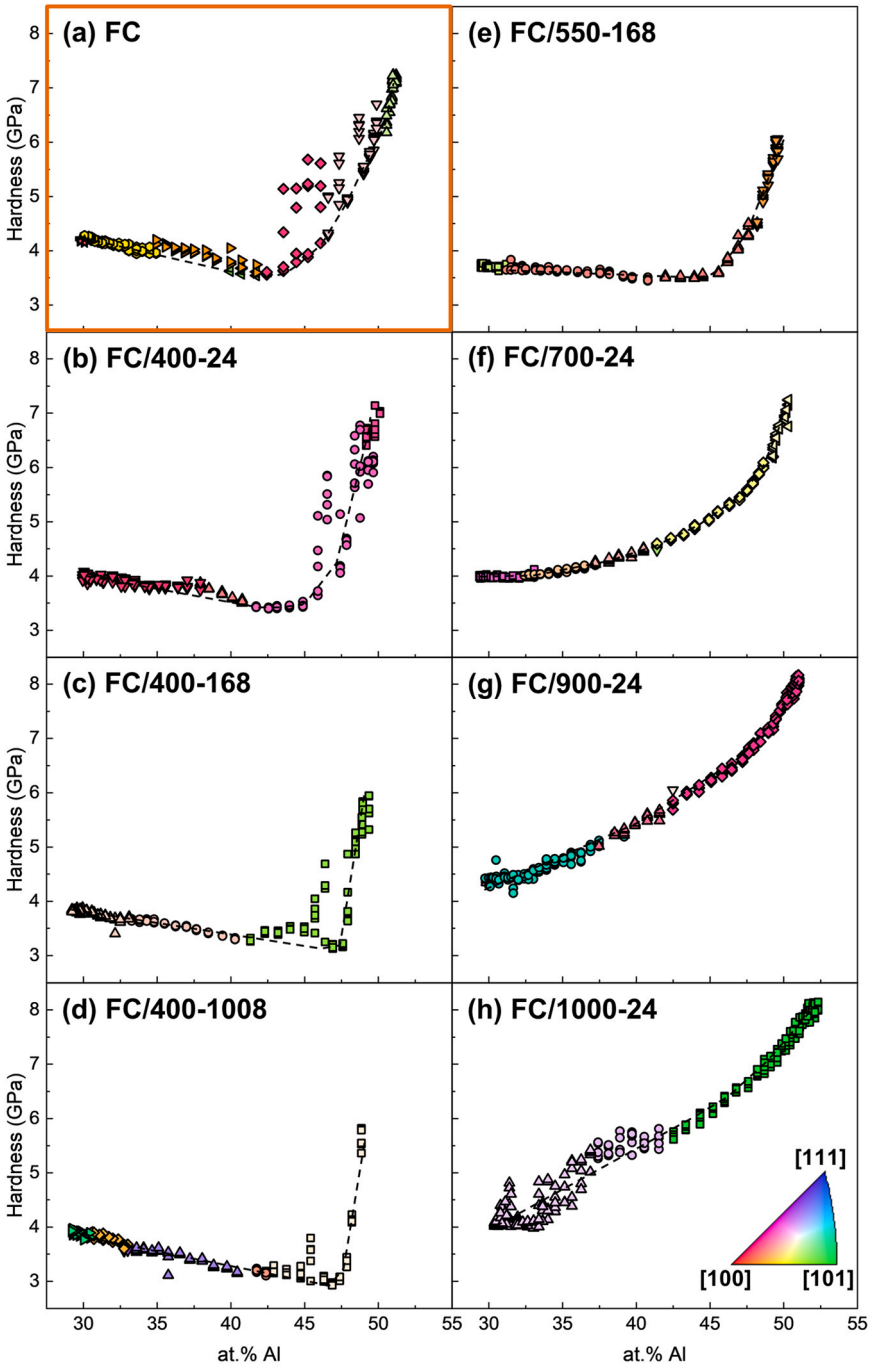

Fig. 4. Variation of hardness with Al content of FeAl for different heat-treatment conditions: (a) FC, (b) FC/400-24, (c) FC/400-168, (d) FC/400-1008, (e) FC/550-168, (f) FC/700-24, (g) FC/900-24, and (h) FC/1000-24. The data points in all the plots are color coded according to the inverse pole figure in (h) to indicate the grain orientation. An orange frame for the FC condition is made to distinguish it from the additional heat-treatment conditions, since it is the only state with slow cooling (while all the others finally were water quenched). Dotted lines are drawn following the respective trend for each figure as a guide for the eye.

in a minimum in the hardness curves. Instead, a continuous increase of the hardness with increasing Al content is observed, exhibiting reduced curvature as temperature increases.

Upon closer inspection of Fig. 4, a significant scatter of the hardness values can be noticed in a restricted composition range at around 45 at. % Al in the case of the FC and the three 400 °C heat-treated diffusion couples (i.e., FC/400–24, FC/400–168, and FC/400–1008). The magnitude of the scatter and the range of compositions over which it occurs reduce with increasing heat-treatment time from FC to HT/400–1008, i.e., as the sample becomes well annealed at lower temperature for longer duration. This phenomenon can probably be attributed to the occurrence of more complex vacancy arrangements (such as divacancies and triple defects, as will be discussed in Section 4) in this composition range, which partially still remain during the slow furnace cooling and after low-temperature heat treatment (400 °C in this case). Furthermore, the indents (see Supplementary Information Fig. S5) exhibit differences in the slip traces around the indents in the same grain. They likely reflect local variations in deformation modulated by vacancies, rather than measurement artifacts.

The hardness values in the composition range where the occurrence of widely spaced fine Fe_3AlC precipitates was observed (i.e., on the Fe-rich side approximately below 36 at.% Al after the low-temperature heat

treatments at 400 and 550 °C) show a smooth curve with a continuous transition to the hardness trend above 36 at.% Al. This implies that the Fe_3AlC precipitates present in the grains of FC/400–24, −168, −1008 and FC/550–24 conditions do not affect the hardness measurements and, therefore, their influence can be neglected here. It should also be noted that the $D0_3$-ordering, which was observed in the low Al composition range of the diffusion couples, has no noticeable additional effect on the hardness curves, which remain continuous without any change in the slope.

Moreover, the grain orientation appears to have only a weak influence on the hardness for all heat-treatment conditions, as reflected in only small changes in the values when switching from one grain to another. This was verified by performing nanoindentation experiments on five single-phase bulk samples with Al concentrations of 30, 35, 42, 47, and 50 at.%, which had been heat treated at 400 °C for 120 h and water quenched. Measurements were performed on at least five differently oriented grains for each alloy (the hardness plots are shown in the Supplementary Information Fig. S6), confirming that the influence of orientation on hardness is negligible for the interpretation of the present results.

3.3.2. *Reduced modulus*

The reduced modulus, as obtained from the nanoindentation experiments is shown in Fig. 5 as a function of the Al content. First, we can

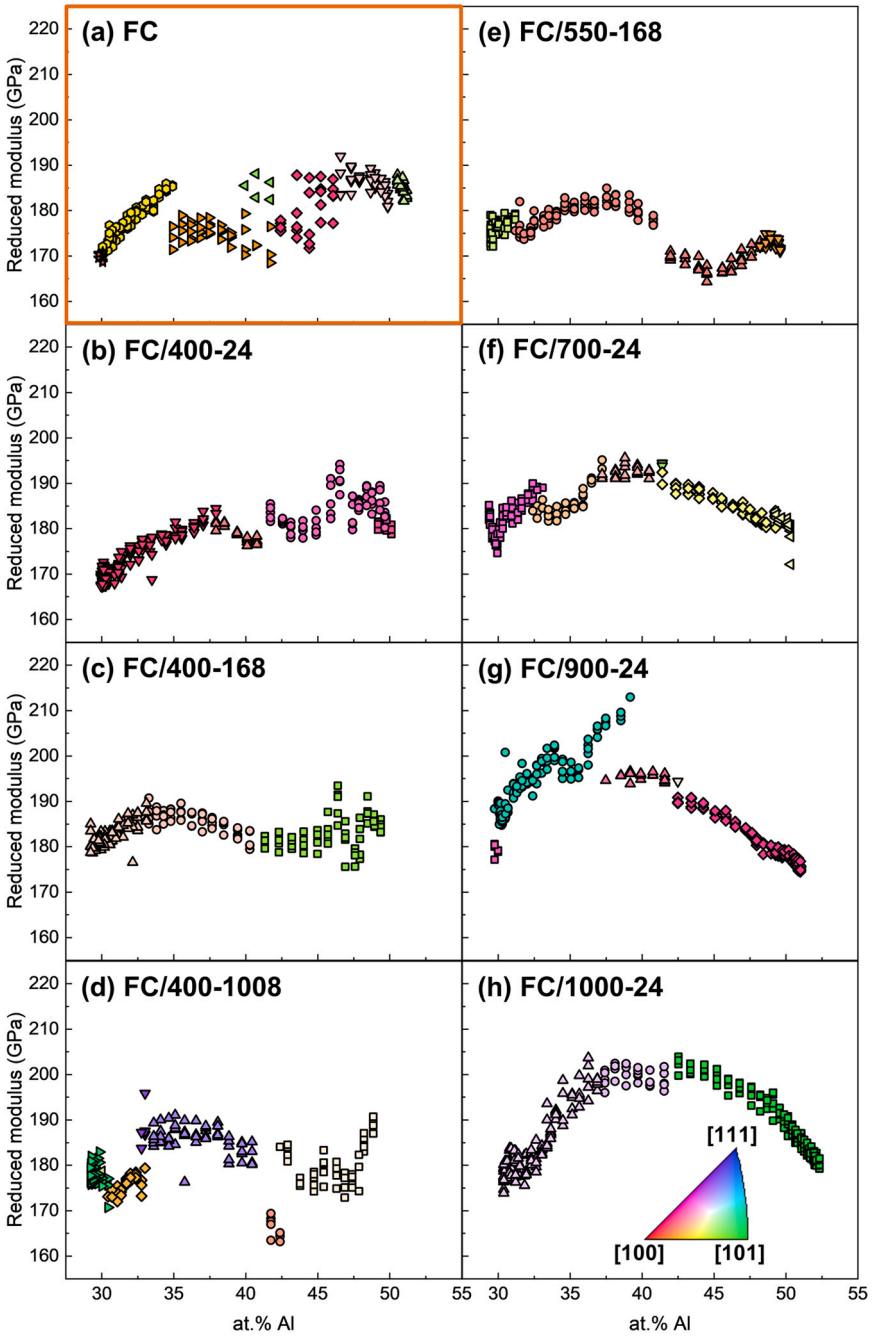

Fig. 5. Variation of reduced modulus with Al content of FeAl for different heat-treatment conditions: (a) FC, (b) FC/400-24, (c) FC/400-168, (d) FC/400-1008, (e) FC/550-168, (f) FC/700-24, (g) FC/900-24, and (h) FC/1000-24. The data points in all the plots are color coded according to the inverse pole figure in (h) to indicate the grain orientation. An orange frame for the FC condition is made to distinguish it from the additional heat-treatment conditions, since it is the only state with slow cooling (while all the others finally were water quenched).

observe the effect of the elastic anisotropy of the B2-ordered phase which manifests itself in steps in the values during the change from one grain to another. From the literature, it is well known that the B2-ordered FeAl is elastically anisotropic [50,51], with $E_{[100]} < E_{[110]} < E_{[111]}$ [61]. This trend is confirmed in the present measurements. For this, the effect of grain orientation on the reduced modulus was also determined separately by performing nanoindentation in differently oriented grains on a bulk Fe-Al alloy with a fixed composition of 50 at.% Al (see Supplementary Information Fig. S7). Despite the discontinuities in the curves of the reduced modulus due to elastic anisotropy, Fig. 5 reveals a clear trend of the reduced modulus as a function of composition. In all cases, there is an initial increase up to a maximum, followed by a decrease irrespective of the heat-treatment condition. The Al content at which the reduced modulus starts to decrease is at about 40–42 at.% Al for the highest heat-treatment temperatures of 900 and 1000 °C. It continuously shifts towards lower concentrations with decreasing temperature (~35 at.% Al for the long-time low temperature heat treatments FC/400–168 and FC/400–1008). After reaching the maximum, the values of the reduced modulus continuously decrease with Al further increasing up to 50 at.% Al for the samples heat treated at 700, 900, and 1000 °C, while for the 400 °C heat-treated diffusion couples, a decrease in reduced modulus at higher concentration is not clearly discernible. Despite the elastic anisotropy, the results indicate that these trends appear to be driven by changes in composition and not by the change in the grain orientations for a given heat treatment. This will be discussed further in Section 4.2.

4. Discussion

4.1. Defect hardening of B2 FeAl

The hardness curves shown in Fig. 4 can be categorized into two groups based on their trends - those showing a monotonous increase and those exhibiting a minimum before the abrupt increase with increasing Al content. They have been plotted separately in Fig. 6. The hardness data of the furnace-cooled condition are included in both diagrams as a reference. It is known from the literature [18,19,31] that vacancy hardening is the most influential strengthening mechanism and that the concentration of vacancies increases with increasing Al content in B2-ordered alloys in the entire composition range. However, the decrease in hardness observed here with increasing Al content up to approximately 43–47 at.% Al after low-temperature heat treatments is inconsistent with this trend and must therefore be attributed to another cause. Since the contribution of APBs and dislocations to strengthening is insignificant in B2-ordered FeAl (see Section 1 with reference to [37–39] and Section 3.1), strengthening by anti-site defects, whose concentration can become very high at low Al contents (e.g., up to 20% at 40 at.% Al [44]), must be considered. Although the strengthening effect of anti-site defects in B2-ordered FeAl is weaker than that of vacancies [18,19], their influence can stand out when the vacancy concentrations are very low (i.e., after slow furnace cooling and low-temperature heat treatment that effectively minimize vacancy hardening) and simultaneously when the anti-site defect concentrations are sufficiently high. Since the concentration of anti-site defects required to compensate the deviation from the ideal stoichiometry increases linearly from 50 at.% Al [44], their contribution to hardening will increase as the Al content decreases. This is exactly what the present experiments show, as indicated with the red arrow in Fig. 6a.

Subtle differences can be observed comparing the four hardness curves in Fig. 6a in the composition range between 30 and 45 at.% Al. While all four curves show an approximately linear decrease with increasing Al content, confirming that hardness is dominated by anti-site defect strengthening under these conditions, clearly noticeable differences remain from the different heat treatments. The hardness values obtained after furnace cooling are the highest and are reduced by the subsequent heat treatments at 400 °C. Extension of the heat-treatment time from 24 to 168 h results in an additional slight reduction of the hardness values, while another extension to 1008 h does not lead to any further clearly discernible change of hardness in the Fe-rich composition range. This suggests that relaxation and annihilation of thermal vacancies was completed after the long-term annealing (more than 168 h), whereas this was not achieved after the slow furnace cooling and the short-time heat treatment (24 h) at 400 °C.

Since the concentration of constitutional vacancies becomes high near the stoichiometric composition [23,24], vacancy hardening dominates beyond the compositions of the minimum and results in an abrupt hardness increase. This phenomenon with the sudden increase in vacancy concentrations at high Al contents can be attributed to the combined effect of a decreasing vacancy formation enthalpy [4,62–64] and simultaneously increasing vacancy migration enthalpy with increasing Al content, which becomes about twice as much as the vacancy formation enthalpy for 50 at.% Al [8]. Therefore, it is increasingly difficult to anneal out the increasing number of thermal vacancies that are retained as the Al concentration approaches stoichiometry. Moreover, due to the fact that forming a vacancy on an Fe site is energetically much more favorable than on an Al site (i.e., the vacancies are mainly Fe vacancies) [30,65], more complex vacancy arrangements such as triple defects and divacancies (see Fig. 1d and e for schematics) can form at high Al contents that may require more energy and time to be annealed out and, therefore, may also be retained after quenching to room temperature [4, 25–27,31]. Hence, the minimum occurs because at a certain composition, vacancy hardening takes over the role of the dominant hardening

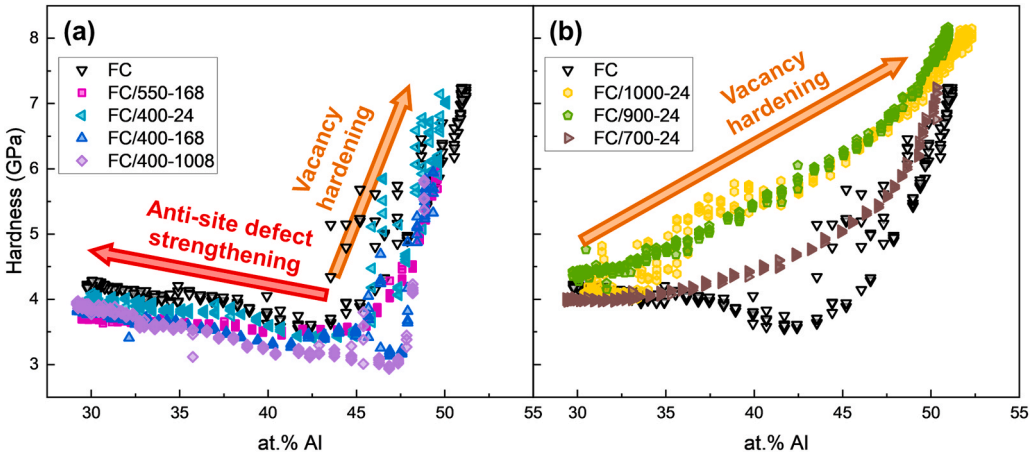

Fig. 6. Variation of hardness as a function of at.% Al plots categorized into two groups: (a) low-temperature heat-treatment conditions, and (b) high-temperature heat-treatment conditions. FC data in both figures are shown as reference.

effect from the anti-site defect hardening. Additionally, the present results show that the Al content corresponding to the minimum hardness shifts to higher Al with increasing heat-treatment time at 400 °C (from 43 to 47 at.% Al between 24 and 1008 h). This is because with increasing time, an increasing amount of vacancies is annealed out. This reduces the contribution of vacancies to the combined hardening effect of vacancies and anti-site atoms (the concentration of which remains more or less unaffected by varying heat-treatment temperatures and times [34]), which results in a shift of the minimum to higher Al contents.

The hardness profiles of the diffusion couples that were heat treated at higher temperatures (700, 900, and 1000 °C) do not show any minima as can be seen in Fig. 6b, which was also previously reported in the literature [16,18]. This implies that the concentrations of quenched-in thermal vacancies are high and the resulting hardening effect is dominant enough to completely mask the influence of the anti-site defects. As expected, the heat treatment at 700 °C produces a lower concentration of thermal vacancies than those at 900 and 1000 °C. The almost overlapping hardness values measured for the diffusion couples heat treated at 900 and 1000 °C indicate that the number of quenchable vacancies is similar for both temperatures.

Despite strengthening by vacancies and anti-site defects which results in varying hardness trends for the different heat treatments, it is intriguing to see that the hardness differences become smaller near the end compositions (30 and 50 at.% Al) and are the largest in between. The hardness values at the Fe-rich end near 30 at.% Al seem to almost converge for all the heat treatments because the contribution of vacancies becomes smaller. With decreasing Al content, the formation enthalpy of vacancies increases [4,62–64] and the amount of vacancies decreases [4,25–27,31], and at the same time their migration enthalpy decreases [8]. Therefore, not only the concentration of vacancies is comparably low (nearly three orders of magnitude lower than at 50 at.% Al [31]), but this concentration can also be influenced to a limited extent by different heat treatments. This explains why hardness values seem to converge at the low-Al end of the curves. To analyze this further, the hardness differences (ΔH) were calculated for FC/550–168, 700–24, and 900–24 with FC/400–1008 as reference and are shown in Fig. 7. We have selected FC/400–1008 as the reference since it represents the most relaxed state in terms of vacancy concentration. Since the concentration of anti-site atoms changes insignificantly under different heat treatments for a specific composition [34], the plots show us the sole effect of vacancy concentration. Although the hardness converges as the composition approaches 30 at.% Al, the hardness of FC/900–24 is the highest ($\Delta H_{FC/900–24\ -\ FC/400–1008} = 0.53$ GPa), followed by FC/700–24 ($\Delta H_{FC/700–24\ -\ FC/400–1008} = 0.15$ GPa), which are the lowest vacancy hardening values for each heat treatment. The ΔH curves of FC/900–24 and FC/700–24 increase up to an Al content of about 47 at.%, where the minimum is reached for FC/400–1008, and then drop drastically. For FC/550–168, ΔH slowly increases from 32.5 at.% Al up to 44 at.% Al and then increases suddenly up to 1.31 GPa and finally drops like the others. This implies that there is a gradual increase in the concentration of vacancies for the lower Al contents (up to 44 at.% Al) and, in the range between 44 and 47 at.% Al, rather high concentrations of vacancies are formed and retained to manifest such a sudden and high difference in hardness. This is in good agreement with the trend of vacancy concentrations as a function of composition reported in the literature [4,18,26,31]. Furthermore, the highest value of hardness is always achieved as the composition approaches 50 at.% Al independent of the heat treatment, because higher concentrations of vacancies are formed, which due to the simultaneous increase in migration enthalpy are difficult to be annealed and, therefore, can be quenched even for the long-time-annealed FC/400–1008 diffusion couple. Therefore, the hardness difference ΔH becomes smaller again near 50 at.% Al as shown in Fig. 7. This particular behavior might also explain the abrupt changes in properties (lattice resistance, Hall Petch slope, brittle-to-ductile transition temperature) [7,11,13] as mentioned in the Introduction.

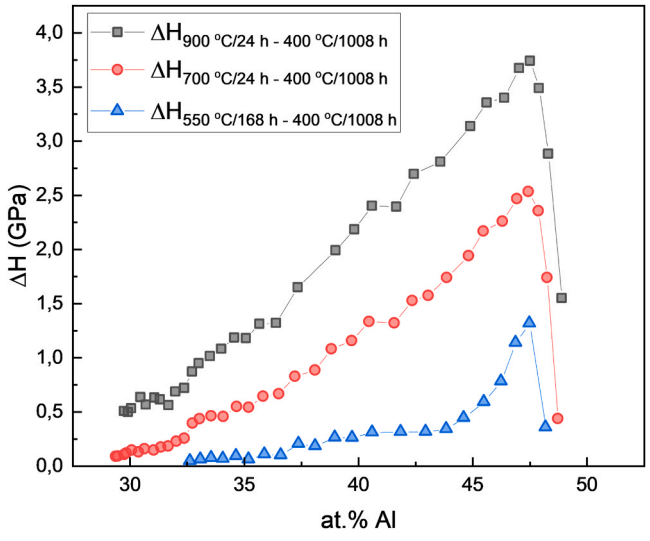

Fig. 7. Hardness difference (ΔH) as a function of at.% Al plotted for FC/900-24, FC/700-24, and FC/550-168 by subtracting FC/400-1008 hardness values (refer to Fig. 4 for original values).

4.2. Trend of reduced modulus

In general, shorter and stronger atomic bonds (such as resulting from covalent and ionic bonding) are stiffer, leading to higher elastic moduli [66,67], and vice versa since the elastic modulus is a measure of the bond stiffness. For B2-ordered FeAl, the Fe and Al atoms form strong directional covalent bonds in addition to the metallic bonding through hybridization of Fe 3d and Al 3sp orbitals [68–70]. Therefore, the weaker metallic bonds (Fe-Fe and Al-Al) are replaced by stronger Fe-Al bonds with Al contents increasing from 30 at.% Al to the stoichiometric composition as the concentration of anti-site atoms decreases. On the other hand, the lattice parameter also increases [18,26,71] owing to the addition of larger Al atoms. These two effects theoretically counter each other, i.e., the overall bonding becomes stronger which leads to a higher elastic modulus and the lattice parameter becomes larger resulting in reduction of the elastic modulus.

The present data obtained from the nanoindentation show that E_r initially increases from 30 at.% Al with increasing Al content as was also observed in other works measuring elastic modulus [12,50–52,72]. However, Köster and Gödecke [52], who measured the elastic modulus of polycrystalline FeAl bulk alloys as a function of composition using a resonance method (Förster elastomat), reported such an increase of the modulus only up to 36 at.% Al followed by a plateau region with only insignificant changes in values beyond 36 at.% Al. Harmouche and Wolfenden [53,54] measured the elastic modulus of FeAl bulk alloys in the composition range 40–49 at.% Al employing a piezoelectric ultrasonic composite oscillator technique. They obtained a concave-shaped (smooth increase and decrease) elastic modulus curve as a function of composition with a maximum occurring near 44 at.% Al. Supporting Harmouche and Wolfenden's measurements, similar concave-shaped curves are observed in the present work for the diffusion couples heat treated at higher temperatures (FC/700–24, FC/900–24, and FC/1000–24). The same trend, i.e., the occurrence of a maximum followed by a decrease, is also exhibited by the rest of the heat treatments, although only for a limited composition range. These experimental observations suggest that the initial increase could be attributed to the dominant influence of the replacement of weaker (metallic) by stronger (directional) bonds, whereas the decrease at higher Al contents can be because of the dominant influence of larger lattice parameter.

Additionally, apart from the changes as a function of composition, the different heat treatments and quenching temperatures also affect the

lattice parameter due to the difference in the concentration of vacancies [18,26]. Quenching from higher-temperature results in lower lattice parameters as higher vacancy concentrations reduce the average volume of the B2 unit cell [26]. In agreement with it, a clear increase in the elastic modulus was observed when comparing a well-annealed alloy (finally annealed at 300 °C and air-cooled) to an alloy water-quenched from 700 °C [12]. Since the effect of heat treatments on the vacancy concentration is stronger at higher Al contents, this might explain why the position of the maximum continuously shifts from 35 to 42 at.% Al, when the heat-treatment temperatures increase from 400 to 1000 °C.

However, the above presented argumentation is still insufficient to give a complete description and interpretation of the complex behavior of the modulus data. For example, Zamanzade *et al.* [47] have reported that the reduced modulus of Fe-30 and 45 at.% Al alloys exhibited a small decrease of 1–3 GPa (~1% change) with increasing quenching temperature, a trend that is not in agreement with the current analysis and other literature [12]. A thorough investigation studying the electronic aspects, bond strength and interatomic distance of FeAl with varying compositions and point defect concentrations using computational methods is required to understand the presented behavior of the elastic modulus in detail. Respective calculation work is currently ongoing and will be presented in a later publication.

5. Conclusions

In the present study, diffusion couples combined with nano-indentation were used to map the hardness and reduced modulus across the entire single-phase B2-ordered FeAl composition range and to separate, as far as possible, the roles of vacancies and anti-site defects by applying a series of different heat treatments at temperatures and duration from 400 to 1000 °C. The findings can be summarized as follows:

1) The diffusion couple technique was successfully applied for the first time to fabricate B2-ordered FeAl samples covering the entire composition range of the phase and to study the role and effects of point defects within a single specimen while maintaining the same low impurity concentrations.
2) At low vacancy concentrations (furnace-cooled or low-temperature heat-treated conditions), hardness on the Fe-rich side of the B2 composition range is mainly controlled by anti-site defect strengthening and shows a non-monotonic dependence with a minimum towards higher Al contents. Vacancy hardening dominates beyond the minimum hardness composition. When quenched from high temperatures, vacancy hardening masks the much weaker effect of anti-site defect strengthening, thereby increasing the hardness monotonically with Al content.
3) Hardness increases steeply near the stoichiometric composition of FeAl due to the high concentration of vacancies arising from the combination of low formation and high migration enthalpies.
4) The reduced modulus exhibits an increase from 30 at.% Al to a maximum followed by a decrease at high Al contents for all heat-treatment conditions. This maximum shifts to higher Al contents for higher heat-treatment temperatures. These trends indicate that an increase of the Al content initially stiffens the lattice by replacing Fe–Fe/Al–Al bonds with stronger Fe–Al bonds as the concentration of anti-site defects decreases, while the decrease of the reduced modulus at higher Al contents might be related to the increasing lattice parameter. In addition, vacancies might contribute to the increase of the elastic modulus by decreasing the lattice parameter. However, the exact interplay between the different effects on the elastic modulus still needs further clarification.

CRediT authorship contribution statement

Jung Soo Lee: Writing – review & editing, Writing – original draft, Visualization, Methodology, Investigation, Formal analysis, Data curation. **Peter Schweizer:** Writing – review & editing, Methodology, Investigation, Formal analysis, Data curation. **Jan Lars Riedel:** Writing – review & editing, Methodology, Investigation, Formal analysis, Data curation. **Martin Heilmaier:** Writing – review & editing, Supervision, Funding acquisition, Conceptualization. **Alexander Kauffmann:** Writing – review & editing, Supervision, Funding acquisition, Conceptualization. **James P. Best:** Writing – review & editing, Supervision, Project administration, Funding acquisition, Conceptualization. **Gerhard Dehm:** Writing – review & editing, Supervision. **Anwesha Kanjilal:** Writing – review & editing, Supervision, Resources, Project administration, Conceptualization. **Frank Stein:** Writing – review & editing, Supervision, Resources, Project administration, Funding acquisition, Conceptualization.

Declaration of Competing Interest

The authors declare that they have no known competing financial interests or personal relationships that could have appeared to influence the work reported in this paper.

Acknowledgements

The financial support by the Deutsche Forschungsgemeinschaft (DFG) within the project “Ermittlung der Ursachen des ungewöhnlichen mechanischen Verhaltens von B2 FeAl” (project number 511095365) is gratefully acknowledged. We gratefully acknowledge Frank Rütters for casting of the alloys, Jürgen Wichert for carrying out the heat treatments of the samples, and Irina Wossack for helping with the EPMA measurements.

Appendix A. Supporting information

Supplementary data associated with this article can be found in the online version at doi:10.1016/j.jallcom.2026.188036.

References

[1] C.T. Liu, E.P. George, P.J. Maziasz, J.H. Schneibel, Recent advances in B2 iron aluminide alloys: deformation, fracture and alloy design, Mater. Sci. Eng. A 258 (1-2) (1998) 84–98, https://doi.org/10.1016/S0921-5093(98)00921-6.
[2] R.R. Judkins, U.S. Rao, Fossil energy applications of intermetallic alloys, Intermetallics 8 (9-11) (2000) 1347–1354, https://doi.org/10.1016/S0966-9795(00)00110-2.
[3] D.G. Morris, M.A. Muñoz-Morris, Recent developments toward the application of iron aluminides in fossil fuel technologies, Adv. Eng. Mater. 13 (1-2) (2011) 43–47, https://doi.org/10.1002/adem.201000210.
[4] M. Zamanzade, A. Barnoush, C. Motz, A review on the properties of iron aluminide intermetallics, Crystals 6 (1) (2016) 10, https://doi.org/10.3390/cryst6010010.
[5] M. Palm, F. Stein, G. Dehm, Iron aluminides, Annu. Rev. Mater. Res. 49 (2019) 297–326, https://doi.org/10.1146/annurev-matsci-070218-125911.
[6] N.I. Polushkin, V. Oliveira, R. Vilar, M. He, M.V. Shugaev, L.V. Zhigilei, Phase-change magnetic memory: rewritable ferromagnetism by laser quenching of chemical disorder in $Fe_{60}Al_{40}$ Alloy, Phys. Rev. Appl. 10 (2) (2018) 024023, https://doi.org/10.1103/PhysRevApplied.10.024023.
[7] I. Baker, P. Munroe, Mechanical properties of FeAl, Int. Mater. Rev. 42 (5) (1997) 181–205, https://doi.org/10.1179/imr.1997.42.5.181.
[8] I. Baker, An Overview of the Mechanical Properties of FeAl, 1128, MRS Online Proceedings Library (OPL), 2008, https://doi.org/10.1557/PROC-1128-U02-01.
[9] F. Stein, Al-Fe (Aluminium-Iron), F. Stein, M. Palm (Eds.), Selected Al–Fe–X Ternary Systems for Industrial Applications, Materials Science International Services GmbH, Stuttgart, Germany, 2022, pp. 1–38. ⟨https://hdl.handle.net/21.11116/0000-000C-15C4-F⟩.
[10] H. Xiao, I. Baker, The relationship between point defects and mechanical properties in Fe - Al at room temperature, Acta Metall. Et. Mater. 43 (1) (1995) 391–396, https://doi.org/10.1016/0956-7151(95)90295-3.
[11] D. Risanti, J. Deges, L. Falat, S. Kobayashi, J. Konrad, M. Palm, B. Pöter, A. Schneider, C. Stallybrass, F. Stein, Dependence of the brittle-to-ductile transition temperature (BDTT) on the Al content of Fe–Al alloys, Intermetallics 13 (12) (2005) 1337–1342, https://doi.org/10.1016/j.intermet.2005.02.007.
[12] E. Frutos, D.G. Morris, M.A. Muñoz-Morris, Evaluation of elastic modulus and hardness of Fe–Al base intermetallics by nano-indentation techniques, Intermetallics 38 (2013) 1–3, https://doi.org/10.1016/j.intermet.2013.02.012.

[13] I. Baker, P. Nagpal, F. Liu, P. Munroe, The effect of grain size on the yield strength of FeAl and NiAl, Acta Metall. Et. Mater. 39 (7) (1991) 1637–1644, https://doi.org/10.1016/0956-7151(91)90251-U.

[14] A. Lawley, Intermetallic Compounds, in: J.H. Westbrook (Ed.), Mechanical Properties - Plastic Behavior, John Wiley and Sons, Inc, 1967, pp. 464–488.

[15] J.H. Westbrook, R.L. Fleischer, Principles, in: Intermetallic Compounds, 1, John Wiley and Sons, Chichester, UK, 1995.

[16] P. Nagpal, I. Baker, Effect of cooling rate on hardness of FeAl and NiAl, Metall. Trans. A 21 (8) (1990) 2281–2282, https://doi.org/10.1007/BF02647891.

[17] E.P. George, I. Baker, Thermal vacancies and the yield anomaly of FeAl, Intermetallics 6 (7-8) (1998) 759–763, https://doi.org/10.1016/S0966-9795(98)00063-6.

[18] Y. Chang, L. Pike, C. Liu, A. Bilbrey, D. Stone, Correlation of the hardness and vacancy concentration in FeAl, Intermetallics 1 (2) (1993) 107–115, https://doi.org/10.1016/0966-9795(93)90028-T.

[19] L.M. Pike, Y.A. Chang, C. Liu, Point defect concentrations and hardening in binary B2 intermetallics, Acta Mater. 45 (9) (1997) 3709–3719, https://doi.org/10.1016/S1359-6454(97)00028-1.

[20] J. Schneibel, Strengthening of iron aluminides by vacancies and/or nickel, Mater. Sci. Eng. A 258 (1-2) (1998) 181–186, https://doi.org/10.1016/S0921-5093(98)00932-0.

[21] J. Jordan, S. Deevi, Vacancy formation and effects in FeAl, Intermetallics 11 (6) (2003) 507–528, https://doi.org/10.1016/S0966-9795(03)00027-X.

[22] M. Morris, O. George, D. Morris, Vacancies, vacancy aggregates and hardening in FeAl, Mater. Sci. Eng. A 258 (1-2) (1998) 99–107, https://doi.org/10.1016/S0921-5093(98)00922-8.

[23] T. Hehenkamp, P. Scholz, B. Köhler, R. Kerl, Vacancy formation and diffusion in FeAl-alloys, Defect Diffus. Forum 194-199 (2001) 389–396, https://doi.org/10.4028/www.scientific.net/DDF.194-199.389.

[24] D. Paris, P. Lesbats, Vacancies in Fe-Al alloys, J. Nucl. Mater. 69-70 (1978) 628–632, https://doi.org/10.1016/0022-3115(78)90297-0.

[25] J. Čížek, F. Lukáč, I. Procházka, R. Kužel, Y. Jirásková, D. Janičkovič, W. Anwand, G. Brauer, Characterization of quenched-in vacancies in Fe–Al alloys, Physica B Condensed Matter 407 (14) (2012) 2659–2664, https://doi.org/10.1016/j.physb.2011.12.122.

[26] M. Kogachi, T. Haraguchi, Quenched-in vacancies in B2-structured intermetallic compound FeAl, Mater. Sci. Eng. A 230 (1-2) (1997) 124–131, https://doi.org/10.1016/S0921-5093(97)00016-6.

[27] T. Haraguchi, M. Kogachi, Point defect behavior in B2-type intermetallic compounds, Mater. Sci. Eng. A 329 (2002) 402–407, https://doi.org/10.1016/S0921-5093(01)01613-6.

[28] J. Mayer, C. Elsässer, M. Fähnle, Concentrations of atomic defects in B2-Fe_xAl_{1-x}. An ab-initio study, Phys. Status Solidi (b) 191 (2) (1995) 283–298, https://doi.org/10.1002/pssb.2221910205.

[29] R. Krachler, H. Ipser, Application of the grand canonical ensemble to the study of equilibrium point defect concentrations in binary intermetallic phases with the B2-structure, Intermetallics 7 (2) (1999) 141–151, https://doi.org/10.1016/S0966-9795(98)00023-5.

[30] H.İ. Sözen, E. Mendive-Tapia, T. Hickel, J. Neugebauer, Ab initio investigations of point and complex defect structures in B2-FeAl, Phys. Rev. Mater. 6 (2) (2022) 023603, https://doi.org/10.1103/PhysRevMaterials.6.023603.

[31] F. Lukáč, J. Čížek, I. Procházka, Y. Jirásková, D. Janičkovič, W. Anwand, G. Brauer, Vacancy-induced hardening in Fe-Al alloys, J. Phys. Conf. Ser. 443 (2013) 012025, https://doi.org/10.1088/1742-6596/443/1/012025.

[32] I. Prochazka, T. Vlasak, J. Cizek, F. Lukac, M. Liedke, W. Anwand, Y. Jiraskova, D. Janickovic, Quenched-in vacancies and hardening of Fe-Al intermetallics, Acta Phys. Pol. A 137 (2) (2020) 255–259, https://doi.org/10.12693/APhysPolA.137.255.

[33] R. Wang, Y. Zhao, Z. Li, H. Chen, X. Tao, Y. Ouyang, The effect of Al content on the structural, mechanical, and thermal properties of B2-FeAl and $D0_3$-Fe_3Al from atomistic study, Mater. Res. Express 5 (2) (2018) 026512, https://doi.org/10.1088/2053-1591/aaabda.

[34] M. Kogachi, T. Haraguchi, Random vacancy distribution in B2-type intermetallic compound FeAl, Scr. Mater. 39 (2) (1998) 159–165, https://doi.org/10.1016/S1359-6462(98)00145-6.

[35] M. Furukawa, Y. Miura, M. Nemoto, Strengthening mechanisms in Al–Li alloys containing coherent ordered particles, Trans. Jpn. Inst. Met. 26 (4) (1985) 230–235, https://doi.org/10.2320/matertrans1960.26.230.

[36] A. Ardell, J. Huang, Antiphase boundary energies and the transition from shearing to looping in alloys strengthened by ordered precipitates, Philos. Magaz. Lett. 58 (4) (1988) 189–197, https://doi.org/10.1080/09500838808214752.

[37] R. Osmundsen, I. Baker, The effect of antiphase boundary tubes on the hardness of FeAl, Metall. Mater. Trans. A 52 (9) (2021) 3694–3698, https://doi.org/10.1007/s11661-021-06355-w.

[38] G. Hillel, E. Galaeva, I. Edry, D. Fuks, M. Pinkas, L. Meshi, Understanding the formation mechanisms and stability of the anti-phase boundaries (APBs) in Al-Fe B2, J. Alloy. Compd. 970 (2024) 172639, https://doi.org/10.1016/j.jallcom.2023.172639.

[39] M. Morris, D. Morris, Quenching and ageing effects on defects and their structures in FeAl alloys, and the influence on hardening and softening, Scr. Mater. 38 (3) (1998) 509–516, https://doi.org/10.1016/S1359-6462(97)00468-5.

[40] M. Kogachi, T. Haraguchi, S. Kim, Point defect behavior in high temperature region in the B2-type intermetallic compound FeAl, Intermetallics 6 (6) (1998) 499–510, https://doi.org/10.1016/S0966-9795(97)00097-6.

[41] K. Yoshimi, S. Hanada, The strength properties of iron aluminides, JOM 49 (8) (1997) 46–49, https://doi.org/10.1007/BF02914403.

[42] N.De Diego, F. Plazaola, J.A. Jiménez, J. Serna, J. del Rıo, A positron study of the defect structures in the $D0_3$ and B2 phases in the Fe–Al system, Acta Mater. 53 (1) (2005) 163–172, https://doi.org/10.1016/j.actamat.2004.09.013.

[43] W. Köster, T. Gödecke, Physikalische Messungen an Eisen-Aluminium-Legierungen mit 10 bis 50 At.-% Al: I. Bestätigung und Ergänzung des Zustandsbildes Eisen-Aluminium, Int. J. Mater. Res. 71 (12) (1980) 765–769, https://doi.org/10.1515/ijmr-1980-711201.

[44] T. Haraguchi, F. Hori, R. Oshima, M. Kogachi, A study of vacancy-type defects in the B2-phase region of the Fe–Al system by positron annihilation method, Intermetallics 9 (9) (2001) 763–770, https://doi.org/10.1016/S0966-9795(01)00061-9.

[45] T. Haraguchi, F. Hori, R. Oshima, M. Kogachi, Defect analysis in B2-type FeAl alloys by positron annihilation measurements at 100 K, Mater. Sci. Forum 363-365 (2001) 201–203, https://doi.org/10.4028/www.scientific.net/MSF.363-365.201.

[46] J. Del Río, N. De Diego, J. Jiménez, C. Gómez, A positron annihilation study of two Fe-Al alloys in the B2 region, Intermetallics 18 (7) (2010) 1306–1309, https://doi.org/10.1016/j.intermet.2010.02.020.

[47] M. Zamanzade, G. Hasemann, C. Motz, M. Krüger, A. Barnoush, Vacancy effects on the mechanical behavior of B2-FeAl intermetallics, Mater. Sci. Eng. A 712 (2018) 88–96, https://doi.org/10.1016/j.msea.2017.11.054.

[48] J. Wolff, M. Franz, A. Broska, B. Köhler, T. Hehenkamp, Defect types and defect properties in FeAl alloys, Mater. Sci. Eng. A 239 (1997) 213–219, https://doi.org/10.1016/S0921-5093(97)00584-4.

[49] J. Ehrler, M.O. Liedke, J. Čížek, R. Boucher, M. Butterling, S. Zhou, R. Böttger, E. Hirschmann, T.T. Trinh, A. Wagner, The role of open-volume defects in the annihilation of antisites in a B2-ordered alloy, Acta Mater. 176 (2019) 167–176, https://doi.org/10.1016/j.actamat.2019.06.037.

[50] P. Mouturat, G. Sainfort, G. Cabane, Module d'elasticite des alliages fer-aluminium en fonction de la temperature et de la teneur en aluminium, J. Nucl. Mater. 21 (2) (1967) 149–157, https://doi.org/10.1016/0022-3115(67)90146-8.

[51] H. Leamy, E. Gibson, F. Kayser, The elastic stiffness coefficients of iron-aluminum alloys—I Experimental results and thermodynamic analysis, Acta Metall. 15 (12) (1967) 1827–1838, https://doi.org/10.1016/0001-6160(67)90047-8.

[52] W. Köster, T. Gödecke, Physikalische Messungen an Eisen-Aluminium-Legierungen mit 10 bis 50 At.-% Al: IV. Der Elastizitätsmodul der Legierungen, Int. J. Mater. Res. 73 (2) (1982) 111–114, https://doi.org/10.1515/ijmr-1982-730208.

[53] M. Harmouche, A. Wolfenden, Modulus measurements in ordered co-al, fe-al, and ni-al alloys, J. Test. Eval. 13 (6) (1985) 424–428, https://doi.org/10.1520/JTE10976J.

[54] M. Harmouche, A. Wolfenden, Temperature and composition dependence of Young's modulus for ordered B2 polycrystalline CoAl and FeAl, Mater. Sci. Eng. 84 (1986) 35–42, https://doi.org/10.1016/0025-5416(86)90220-X.

[55] J. Cohron, Y. Lin, R. Zee, E. George, Room-temperature mechanical behavior of FeAl: effects of stoichiometry, environment, and boron addition, Acta Mater. 46 (17) (1998) 6245–6256, https://doi.org/10.1016/S1359-6454(98)00254-7.

[56] J.L. Riedel, A. Kauffmann, S. Guth, M. Muench, G. Winkens, D. Schliephake, J. S. Lee, J.P. Best, F. Stein, M. Heilmaier, Re-assessment of temperature-dependent strength, strain hardening, and deformation behavior in binary Fe–Al intermetallics, Intermetallics 193 (2026) 109273, https://doi.org/10.1016/j.intermet.2026.109273.

[57] W.C. Oliver, G.M. Pharr, An improved technique for determining hardness and elastic modulus using load and displacement sensing indentation experiments, J. Mater. Res. 7 (6) (1992) 1564–1583, https://doi.org/10.1557/JMR.1992.1564.

[58] J. Herrmann, G. Inden, G. Sauthoff, Microstructure and deformation behaviour of iron-rich iron-aluminium alloys with ternary carbon and silicon additions, Steel Res. Int. 75 (5) (2004) 343–352, https://doi.org/10.1002/srin.200405965.

[59] K. Durst, B. Backes, M. Göken, Indentation size effect in metallic materials: correcting for the size of the plastic zone, Scr. Mater. 52 (11) (2005) 1093–1097, https://doi.org/10.1016/j.scriptamat.2005.02.009.

[60] K. Durst, B. Backes, O. Franke, M. Göken, Indentation size effect in metallic materials: modeling strength from pop-in to macroscopic hardness using geometrically necessary dislocations, Acta Mater. 54 (9) (2006) 2547–2555, https://doi.org/10.1016/j.actamat.2006.01.036.

[61] L. Song, X. Tian, H. Jiang, W. Yu, Z. Zhao, H. Zheng, J. Qin, X. Lin, Vacancies effect on the mechanical properties in B2 FeAl intermetallic by the first-principles study, Philos. Magaz. 99 (21) (2019) 2703–2717, https://doi.org/10.1080/14786435.2019.1638529.

[62] J. Rivière, J. Grilhé, Energie de formation des lacunes dans les alliages Fe-Al ordonnes de type B2, Scr. Metall. 9 (9) (1975) 967–970, https://doi.org/10.1016/0036-9748(75)90553-0.

[63] H.-E. Schaefer, K. Frenner, R. Würschum, High-temperature atomic defect properties and diffusion processes in intermetallic compounds, Intermetallics 7 (3-4) (1999) 277–287, https://doi.org/10.1016/S0966-9795(98)00121-6.

[64] M. Zhao, K. Yoshimi, K. Maruyama, K. Yubuta, Thermal vacancy behavior analysis through thermal expansion, lattice parameter and elastic modulus measurements of B2-type FeAl, Acta Mater. 64 (2014) 382–390, https://doi.org/10.1016/j.actamat.2013.10.051.

[65] C. Fu, Y.-Y. Ye, M. Yoo, K. Ho, Equilibrium point defects in intermetallics with the B2 structure: NiAl and FeAl, Phys. Rev. B 48 (9) (1993) 6712, https://doi.org/10.1103/PhysRevB.48.6712.

[66] E. Gao, X. Yuan, S.O. Nielsen, R.H. Baughman, Exploring the bounds on the Young's modulus and gravimetric Young's modulus, Phys. Rev. Appl. 18 (1) (2022) 014044, https://doi.org/10.1103/PhysRevApplied.18.014044.

[67] E. Isotta, W. Peng, A. Balodhi, A. Zevalkink, Elastic moduli: a tool for understanding chemical bonding and thermal transport in thermoelectric

materials, Angew. Chem. 135 (12) (2023) e202213649, https://doi.org/10.1002/ange.202213649.
[68] G. Botton, G. Guo, W. Temmerman, C. Humphreys, Experimental and theoretical study of the electronic structure of Fe, Co, and Ni aluminides with the B2 structure, Phys. Rev. B 54 (3) (1996) 1682, https://doi.org/10.1103/PhysRevB.54.1682.
[69] C.L. Fu, M. Yoo, Deformation behavior of B2 type aluminides: FeAl and NiAl, Acta Metall. Et. Mater. 40 (4) (1992) 703–711, https://doi.org/10.1016/0956-7151(92)90012-4.
[70] Y. Liu, X. Chong, Y. Jiang, R. Zhou, J. Feng, Mechanical properties and electronic structures of Fe-Al intermetallic, Physica B Condensed Matter 506 (2017) 1–11, https://doi.org/10.1016/j.physb.2016.10.032.
[71] A. Taylor, R.M. Jones, Constitution and magnetic properties of iron-rich iron-aluminum alloys, J. Phys. Chem. Solids 6 (1) (1958) 16–37, https://doi.org/10.1016/0022-3697(58)90213-0.
[72] M. Yamamoto, S. Taniguchi, The density, magnetic properties, Young's modulus, and dE-effect, and their change due to quenching in ferromagnetic iron-aluminium alloys. II: Young's modulus and the dE-effect, Sci. Rep. Res. Inst. Tohoku Univ. Ser. A Phys. Chem. Metall. 8 (1956) 193–204, https://doi.org/10.50974/00041852.